Crustal melt granites and migmatites along the Himalaya: melt source, segregation, transport and granite emplacement mechanisms

M. P. Searle, J. M. Cottle*, M. J. Streule and D. J. Waters

Department of Earth Sciences, Oxford University, Parks Road, Oxford OX1 3PR, UK

*Current address: Department of Earth Sciences, University of California, Santa Barbara, CA 93106, USA

ABSTRACT: India–Asia collision resulted in crustal thickening and shortening, metamorphism and partial melting along the 2200 km-long Himalayan range. In the core of the Greater Himalaya, widespread *in situ* partial melting in sillimanite+K-feldspar gneisses resulted in formation of migmatites and Ms+Bt+Grt+Tur ± Crd ± Sil leucogranites, mainly by muscovite dehydration melting. Melting occurred at shallow depths (4–6 kbar; 15–20 km depth) in the middle crust, but not in the lower crust. $^{87}Sr/^{86}Sr$ ratios of leucogranites are very high (0·74–0·79) and heterogeneous, indicating a 100% crustal protolith. Melts were sourced from fertile muscovite-bearing pelites and quartzo-feldspathic gneisses of the Neo-Proterozoic Haimanta–Cheka Formations. Melting was induced through a combination of thermal relaxation due to crustal thickening and from high internal heat production rates within the Proterozoic source rocks in the middle crust. Himalayan granites have highly radiogenic Pb isotopes and extremely high uranium concentrations. Little or no heat was derived either from the mantle or from shear heating along thrust faults. Mid-crustal melting triggered southward ductile extrusion (channel flow) of a mid-crustal layer bounded by a crustal-scale thrust fault and shear zone (Main Central Thrust; MCT) along the base, and a low-angle ductile shear zone and normal fault (South Tibetan Detachment; STD) along the top. Multi-system thermochronology (U–Pb, Sm–Nd, ^{40}Ar–^{39}Ar and fission track dating) show that partial melting spanned ~24–15 Ma and triggered mid-crustal flow between the simultaneously active shear zones of the MCT and STD. Granite melting was restricted in both time (Early Miocene) and space (middle crust) along the entire length of the Himalaya. Melts were channelled up via hydraulic fracturing into sheeted sill complexes from the underthrust Indian plate source beneath southern Tibet, and intruded for up to 100 km parallel to the foliation in the host sillimanite gneisses. Crystallisation of the leucogranites was immediately followed by rapid exhumation, cooling and enhanced erosion during the Early–Middle Miocene.

KEY WORDS: Channel flow, crustal melting, granite emplacement, Himalaya, leucogranite, migmatite, shear zones.

The collision of the Indian plate passive continental margin with the southern active continental margin of Asia (Karakoram in the west; Lhasa block in Tibet) is an ongoing process that started in the Palaeocene. Final marine sedimentation along the Indus–Yarlung Tsangpo suture zone was Early Eocene (49–50·5 Ma) and crustal thickening and shortening by folding and thrusting propagated southward across the north Indian plate margin (Searle *et al*. 1988, 1990, 1997; Rowley 1996; Zhu *et al*. 2005). Since the collision, India has continued to converge and penetrate north into Asia, resulting in double normal thickness continental crust both along the Indian plate margin (Himalaya) and along the south Asian margin (Karakoram–Lhasa Block).

The Himalayan upper crust (Tethyan Himalaya) is composed of folded and thrust Phanerozoic (Late Precambrian to Eocene) sedimentary rocks bounded along the north by the Indus–Tsangpo suture zone and along the south by the South Tibetan detachment (STD), a low-angle, north-dipping normal fault (Burg 1983; Hodges 2000; Cottle *et al*. 2007). South of this the Greater Himalayan Sequence (GHS) is composed of regional Barrovian facies metamorphic rocks, migmatites and leucogranites, bounded along the south by a 2–4 km-thick zone of inverted metamorphic isograds (from sillimanite–kyanite down to biotite–chlorite) with a brittle thrust fault along the base, the Main Central thrust (MCT) zone (Searle *et al*. 2008; Figs. 1, 2). The Lesser Himalaya to the south is composed of underthrust Indian plate rocks including Proterozoic basement and thin Palaeozoic cover sedimentary rocks. The deeper, unexposed lower crust beneath the Himalaya is thought to be underthrust granulite facies Indian shield rocks (Searle *et al*. 2006; Jackson *et al*. 2008). Since the Moho steepens northwards from ca. 40 km depth beneath the Himalayan foreland to ca. 80 km beneath southern Tibet (Schulte-Pelkum *et al*. 2005), or even 90 km beneath the Karakoram–west Tibet (Rai *et al*. 2006), these Precambrian granulites may have undergone a phase transition to eclogite facies rocks during the late Tertiary–present day (Searle *et al*. 2006).

Deep seismic profiling, combined with broadband earthquake and magnetotelluric data across southern Tibet suggest that a high-conductivity layer at 15–20 km-depth reflect partial melting in the middle crust of southern Tibet today (Nelson *et al*. 1996; Wei *et al*. 2001). 'Bright spots' of high electrical conductivity probably reflect pockets of leucogranite magmas forming today at similar P–T conditions and depth as the

© 2009 The Royal Society of Edinburgh. doi:10.1017/S175569100901617X
https://doi.org/10.1017/S175569100901617X Published online by Cambridge University Press

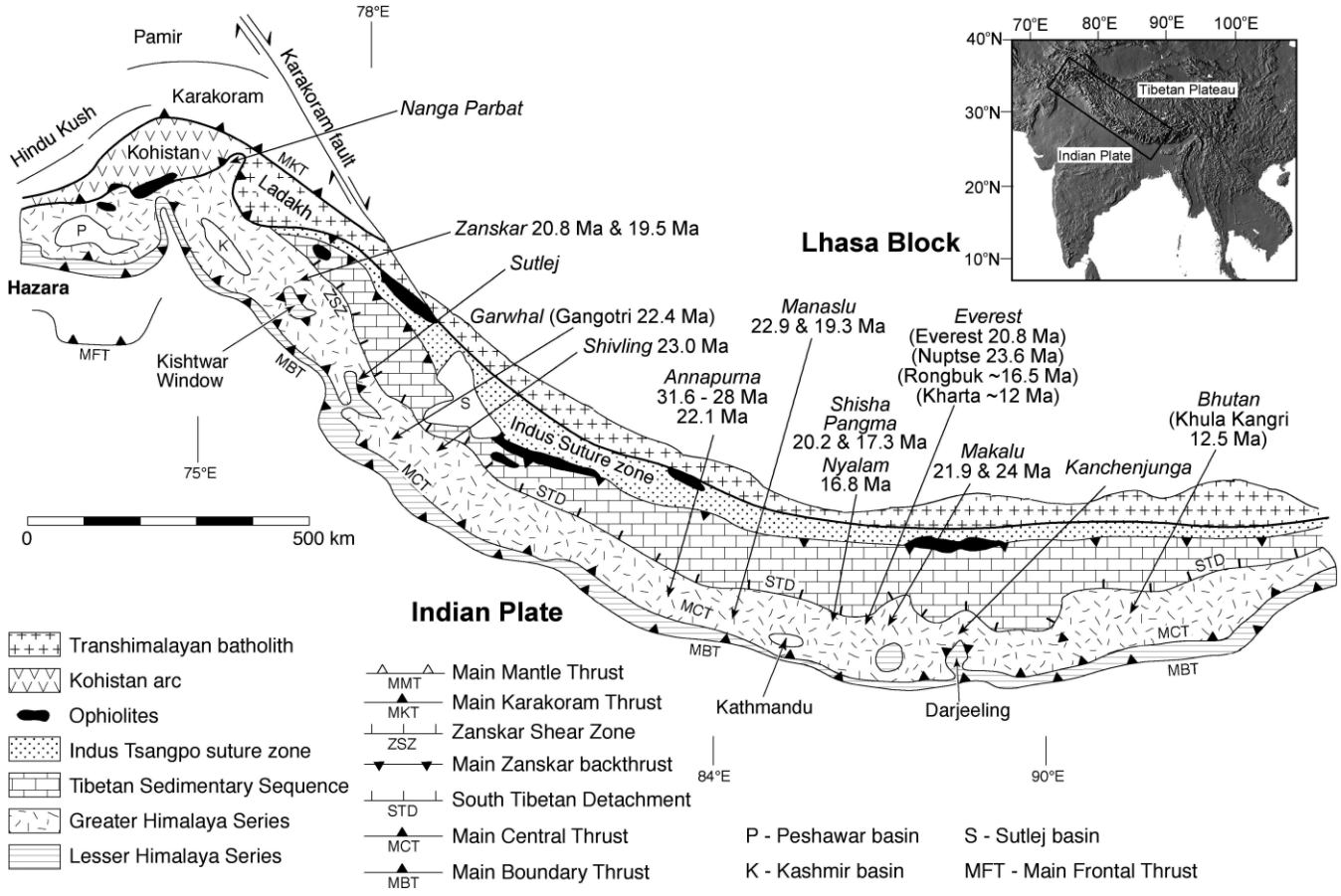

Figure 1 Geological map of the Himalaya showing U–(Th)–Pb ages along the orogen. See text and Godin *et al.* (2006) for sources of data.

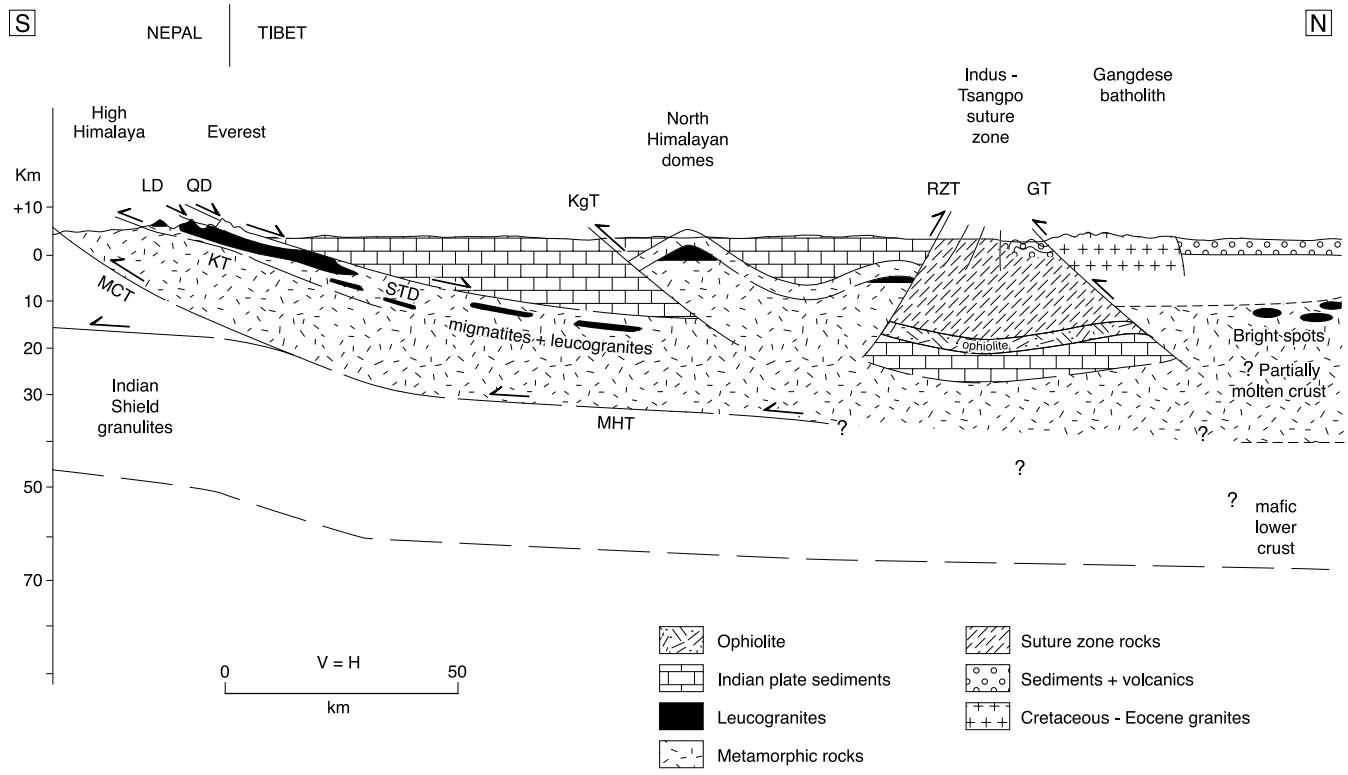

Figure 2 Cross-section across the Everest Himalaya, based on surface geological mapping combined with deep crust seismic constraints from INDEPTH (Nelson *et al.* 1996).

Miocene leucogranites along the Himalaya (Gaillard *et al.* 2004). Seismic reflectors bounding this mid-crustal zone of partial melting can be traced to the ca. 20–16 Ma MCT and STD shear zones along the Greater Himalaya (Hauck *et al.* 1998; Searle *et al.* 2006). Seismic tomographic studies suggest that southern Tibet and the Himalaya are underlain by cold,

https://doi.org/10.1017/S175569100901617X Published online by Cambridge University Press

strong upper mantle attached to the underthrusting Indian shield (Tilmann *et al.* 2003).

Following the India–Asia collision, crustal thickening and shortening (by folding and thrusting) along the northern margin of India resulted in increased pressure and temperatures. Progressive metamorphism evolved with time and in space from initial UHP coesite–eclogite-grade affecting only the leading margin of the Indian plate, to regional kyanite- and sillimanite-grade Barrovian metamorphism affecting most of the GHS and North Himalayan domes. During the Early Miocene increasing temperature and decreasing pressure resulted in decompression melting within the upper part of the middle crust of the Himalaya. One of the most spectacular results of the Himalayan collision was the formation of crustal melt leucogranites from a widespread migmatitic partial melt zone in the middle crust. Many of the highest peaks of the Greater Himalaya are composed of these anatectic granites (e.g. Shivling, Bhagirathi, Thalay Sagar, Manaslu, Makalu, Shisha Pangma, Kangchenjunga, the base of the Everest–Nuptse–Lhotse massif, Chomolhari and Masang Kang).

Since the major shear zones, faults and fabrics across the Himalaya dip to the north and many of the major river drainage access routes run north–south, it is possible to map out a three-dimensional view of the entire middle and upper crust. Thus the Himalaya is a unique orogen where it is possible to trace granitic melts from their mid-crustal source to their present high structural level. This paper reviews the field relationships, metamorphic history and chronology of metamorphism, melting and deformation along the Himalaya. The protolith source of leucogranite melts is discussed, and the partial melting process and melt reactions. These data are used to propose a model for the generation and emplacement of Himalayan leucogranites from source to high structural level, and discuss the role of partial melting and leucogranite formation in the Channel Flow model (Beaumont *et al.* 2001; Grujic *et al.* 2002; Searle *et al.* 2003, 2006; Searle & Szulc 2005; Jessup *et al.* 2006; Law *et al.* 2006).

1. Review of metamorphic history of the Himalaya

The thermal history of the Himalaya involves four 'stages' during part of a 50 m.y. continuum: (1) eclogite metamorphism during initial crustal subduction of the leading edge of India to UHP depths (27·5 kbar; >100 km depth; 720–770 °C) at 46·4 Ma (U–Pb, zircon, allanite; Parrish *et al.* 2006); (2) crustal thickening resulted in peak kyanite grade metamorphism (550–680 °C; 9–11 kbar) at ca. 37–30 Ma (U–Pb, monazite and Sm–Nd garnet ages; Walker *et al.* 1999; Vance & Harris 1999); followed by (3) widespread sillimanite grade metamorphism (620–770 °C; 4·5–7 kbar) accompanied by partial melting and leucogranite formation at ca. 23–16 Ma (Noble & Searle 1995; Walker *et al.* 1999; Simpson *et al.* 2000; Viskupic & Hodges 2001). Burial and thickening, followed by heating, decompression, partial melting and rapid exhumation and cooling resulted in clockwise P–T–t paths (e.g. Hubbard 1989; Searle *et al.* 1999a, b; Hodges 2000; Walker *et al.* 2001; Jamieson *et al.* 2004; Fig. 3). Himalayan eclogite metamorphism is only known so far for certain from Kaghan, North Pakistan and Tso Morari, Ladakh, although it could have occurred elsewhere along the leading margin of the Indian plate and still remain unexposed. In North Pakistan the UHP metamorphism and the medium P–T metamorphic events were probably synchronous and juxtaposed by later thrusting (Treloar *et al.* 2003). The kyanite and sillimanite grade metamorphic events are common along the entire length of the GHS. A fourth Himalayan metamorphic event, characterised

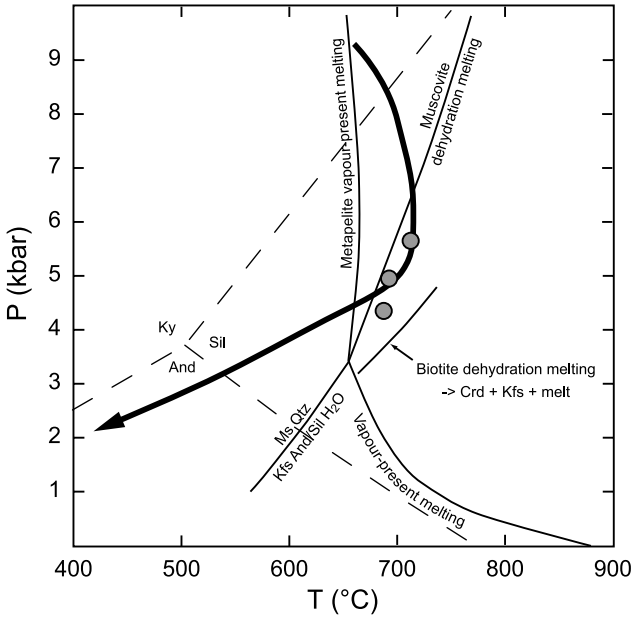

Figure 3 Pressure–temperature diagram showing key equilibria and P–T paths relevant to melting in the GHS. Filled circles are P–T conditions determined for migmatites in the Khumbu Valley, Everest region, from Searle *et al.* (2003). Bold arrowed curve is the P–T path determined for the migmatitic core of the GHS in the Zanskar Himalaya, from Searle *et al.* (1999a). Curves for significant metamorphic and melting reactions in muscovite- and biotite-bearing schists are based on the calculated phase diagram for 'average pelite' in White *et al.* (2001).

by low-P high-T metamorphism, metasomatism and generation of cordierite-bearing leucogranites, has only been recorded in the NW Himalayan syntaxis at Nanga Parbat (Whittington *et al.* 1998, 1999; Zeitler *et al.* 2001a, b; Crowley *et al.* 2009) and the NE Himalayan syntaxis at Namche Barwa (Booth *et al.* 2004).

Himalayan leucogranites were generated during the Early Miocene along the entire 2200 km length of the Greater Himalaya. Crustal melting occurred at relatively shallow depths of ca. 15–20 km depth, and granites were generated from a widespread partial melting migmatite zone in the middle crust. Many Himalayan leucogranites remain more-or-less *in situ* within the sillimanite–K-feldspar migmatite zone and have been exposed only because of underthrusting of successive thrust slices beneath, and subsequent hanging-wall uplift and erosion. Where melt migration has occurred, kilometre-scale, foliation-parallel sill complexes within the upper part of the GHS have transported magma horizontally or along very shallow north-dipping melt channels. No leucogranites cut up across the South Tibetan Detachment (e.g. Murphy & Harrison 1999; Searle & Godin 2003). U–(Th)–Pb ages of leucogranites have been used to constrain timing of motion along the ductile shear zone and the STD low-angle normal fault according to whether the leucogranites are pre-, syn- or post-kinematic with relation to the ductile fabric and brittle fault (e.g.: Searle *et al.* 1997, 2003, 2006).

In Nanga Parbat, Proterozoic granulite basement gneisses were rehydrated to amphibolite before undergoing Oligocene–Miocene metamorphism and at least four phases of melting. The youngest of these was Pleistocene and associated with a vigorous hydrothermal system (Zeitler *et al.* 2001a, b). Cordierite–K-feldspar–quartz pods and veins (Butler *et al.* 1997; Whittington *et al.* 1998, 1999; Whittington & Treloar 2002; Crowley *et al.* 2009) intrude along vertical extensional fractures in the core region of the Nanga Parbat massif. Cordierite occurs as coronas around Al and Fe–Mg rich

https://doi.org/10.1017/S175569100901617X Published online by Cambridge University Press

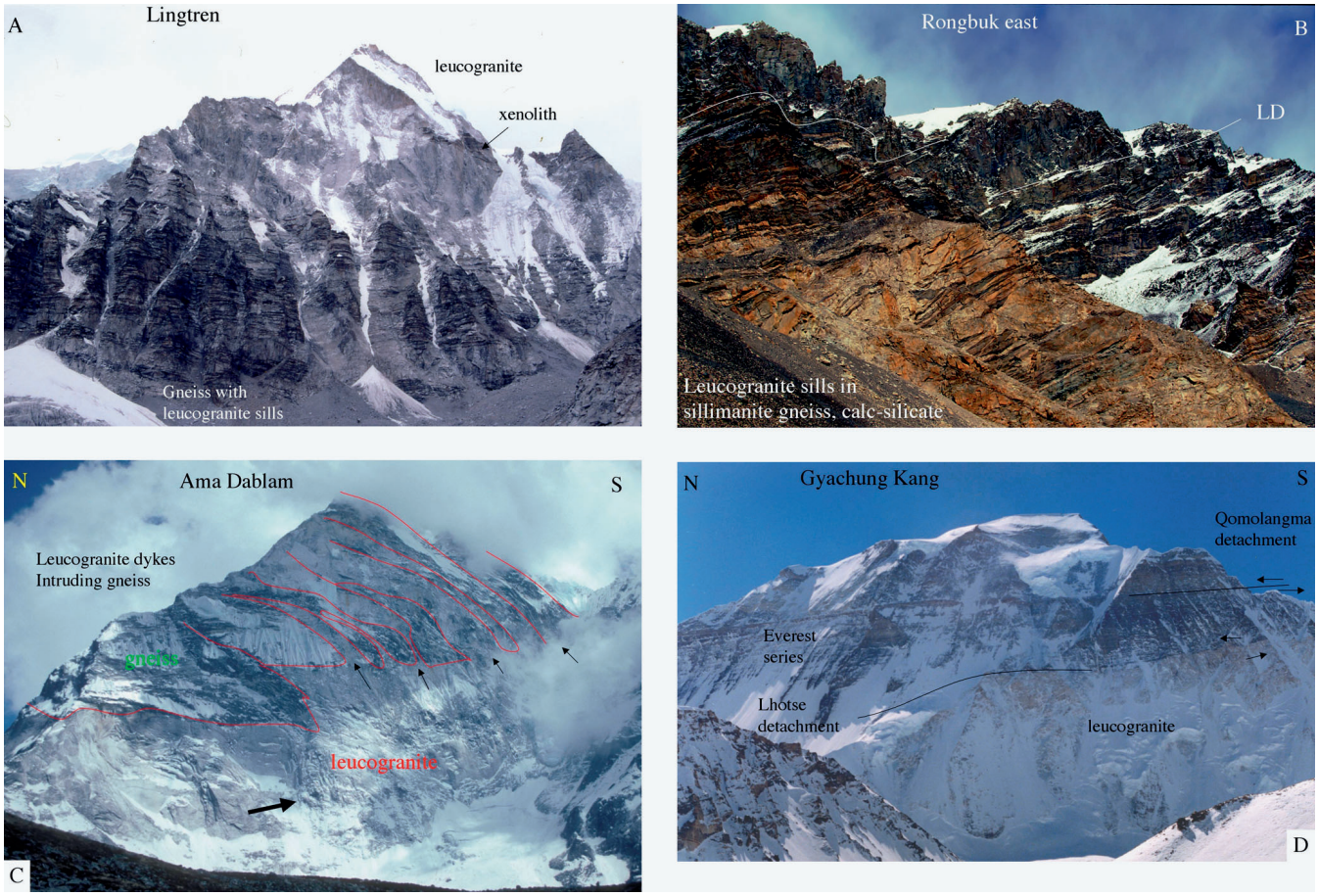

Figure 4 (a) South face of Lingtren (6749 m) showing a 3–4 km-thick sheeted sill complex of horizontally-layered leucogranite with a massive sill at the top enclosing rafts of sillimanite gneiss. (b) Layered leucogranites interlayered with GHS gneisses along footwall of the STD in the Rongbuk valley, north of Everest, south Tibet. (c) North face of Ama Dablam (6828 m) showing leucogranite sheets or thick sills with horizontal dykes bent to the north along the footwall of the STD. (d) Gyachung Kang (7922 m), west of Everest, showing the two low-angle normal faults, the upper Qomolangma detachment and the lower Lhotse detachment.

material which are probably small restitic enclaves. The coronas merge into coarse-grained cordierite in the presence of melt. The development of cordierite-bearing corona assemblages should reflect the final interaction between melt and solid at a time no earlier than that recorded by the crystallisation age of accessory phases in the leucosome. P–T conditions of cordierite coronas from the core of Nanga Parbat are 3·7–4·2 kbar at 700–720°C (Crowley *et al.* 2009). U–Th–Pb ages from monazites and xenotimes in leucogranites give ages as young as 0·76–0·71 Ma (Bowring *et al.* 2004; Crowley *et al.* 2005, 2009). Exhumation rates could be as high as 1·5–2 cm/yr, and 13–15 km of overburden has been eroded from the summit region of Nanga Parbat in less than one million years. In the Eastern Himalayan syntaxis at Namche Barwa, U–Pb SHRIMP zircon ages show the standard 25–18 Ma Himalayan melt events, but also a younger period of 10–3 Ma in the core of the massif (Booth *et al.* 2004), similar to the Nanga Parbat syntaxis.

2. Field relationships of Himalayan granites

Himalayan leucogranites are almost entirely found within the upper part of the Greater Himalayan mid-crustal slab, within the sillimanite+K-feldspar migmatite zone, or intruded along giant sill complexes beneath the STD. Similar field relationships are seen along the entire length of the Himalaya from Zanskar (e.g. Searle *et al.* 1999a; Walker *et al.* 1999; Dezes *et al.* 1999) through Garhwal (e.g. Scaillet *et al.* 1990, 1995; Searle *et al.* 1999b) to Nepal (e.g. Searle & Godin 2003), Sikkim (e.g. Searle & Szulc 2005) and Bhutan (e.g. Grujic *et al.* 2002). Although early studies suggested that the Manaslu leucogranite was an exception by intruding across the STD into the overlying base of the Tethyan sediments (e.g. LeFort 1975, 1981; Guillot *et al.* 1995; Harrison *et al.* 1999), Searle & Godin (2003) showed that the granite was emplaced into high-grade metamorphic rocks beneath the STD, and does not intrude across the STD. The metamorphism around the Manaslu granite is clearly continuous with the regional GHS metamorphism well away from the granite (Searle & Godin 2003), and not contact metamorphism around the granite (Guillot *et al.* 1995).

In the Everest area almost all leucogranites are layer-parallel sills of thicknesses varying from <1 m to 3–4 km (Searle 1999a, b, 2003, 2007; Searle *et al.* 2003, 2006; Jessup *et al.* 2006, 2008; Cottle *et al.* 2007, 2009). The sills can be traced in the field for up to 40 km horizontally across strike, within the upper part of the GHS from the upper Khumbu glacier in Nepal and along the Rongbuk glacier in Tibet (Searle *et al.* 2003, 2006; Jessup *et al.* 2006, 2008; Cottle *et al.* 2007, 2009). Massive horizontal sill complexes make up the upper part of the GHS, with the larger sills reaching 3–4 km thick. The massive granite sheet exposed around the base of the Everest massif is continuous west to Lingtren (Fig. 4a) Pumori, Gyachung Kang and Cho Oyu, east to the granites surrounding the upper Kangshung valley and the base of Makalu, and south to the ballooning Nuptse granite (Searle 1999a, b, 2003, 2007; Jessup *et al.* 2006, 2008). At Rongbuk, early folded and later foliation-parallel sills decrease in abundance up-section to the Lhotse

https://doi.org/10.1017/S175569100901617X Published online by Cambridge University Press

detachment (Fig. 4b), above which a prominent band of calc-silicate truncates the rocks beneath. The brittle Qomolangma detachment above the calc-silicate band and the Everest series pelites then dips north beneath the Tibetan plateau some 35–40 km north of Everest (Cottle *et al*. 2007). Vertical dykes feed magma up from lower sills to higher sills. The highest dykes have been bent around to the north along the footwall of the Lhotse detachment (e.g. on the north face of Ama Dablam; Fig. 4c). West of Mount Everest on Gyachung Kang (Fig. 4d) there are clearly two low-angle detachments, the first of which separates the Cambro-Ordovician sedimentary rocks on the summits from the Everest series greenschist–lower amphibolite facies metapelites and calcschists (Qomolangma detachment) and the second is the lower ductile Lhotse detachment which separates the Everest series above from sillimanite gneisses with abundant leucogranites beneath (Searle 1999a, b, 2003; Searle *et al*. 2003, 2006; Jessup *et al*. 2006, 2008). At deeper structural levels the melting zone, represented by the migmatites, shows layered or stromatic migmatites with *in situ* melts sweating out of quartzo-feldspathic or K-feldspar augen gneisses.

The Manaslu leucogranite in central Nepal is one of the larger Himalayan granites, being ca. 5 km thick (Fig. 5a). The upper margin of the granite is an abrupt fault-bounded contact that corresponds to the Phu detachment, the upper brittle STD normal fault (Searle and Godin 2003) that places Cambrian sedimentary rocks directly above the granite (Fig. 5b). The leucogranite contains rafts of the migmatitic gneiss from which it was apparently derived (Fig. 5c). Tourmaline is a common mafic phase within the Manaslu granite that also contains abundant muscovite, some biotite and garnet (Fig. 5d). Common textures include tourmaline + quartz 'ghosts' that form circular pods of metasomatic late mineral growth associated with boron-rich fluids (Fig. 5e). The stromatic migmatites and early leucogranite melts are cut by later dykes of leucogranite fed by later melting episodes deeper in the crust (Fig. 5f).

Most Himalayan leucogranite bodies are made up of a variety of two-mica ± tourmaline ± garnet leucogranite. Cordierite is uncommon in most Himalayan leucogranites, but it is widespread in the Makalu area, east of Everest, as well as in the younger Pliocene–Recent Nanga Parbat migmatitic leucosomes and very young leucogranite melts (Whittington *et al*. 1998; Bowring *et al*. 2004; Crowley *et al*. 2005, 2009). On Makalu the youngest intrusive phase is a 3 km-thick sill-like body of cordierite granite (Fig. 6a, b) that is fed by a 10 m-wide vertical dyke that cuts across earlier fabrics and older two mica tourmaline leucogranite sills (Fig. 6c). Cordierite occurs as large pale green crystals that are interpreted as a low-pressure (<5 kbar) peritectic phase formed as a product of the biotite dehydration reaction (Fig. 6d). In the Makalu area multiple dykes record at least six episodes of crustal melting in batches (Fig. 6e, f).

3. Review of the U–Th–Pb ages of Himalayan granites

The first attempts to date the crystallisation age of Himalayan leucogranites utilised the $^{87}Sr/^{86}Sr$ method (e.g. Deniel *et al*. 1987). However, the highly variable $^{87}Sr/^{86}Sr$ ratios made calculating ages by this method problematic. Most subsequent age determinations have therefore relied on the U(–Th)–Pb technique. This method is not without its problems however. Because anatexis occurred under low-T conditions, and the resulting melts are highly peraluminous, xenocrystic accessory phases are common. Most have inherited zircon; some have inherited monazite (Copeland *et al*. 1988); whilst inherited xenotime, although rare, is known (Viskupic & Hodges 2001). An additional problem is that monazite, the mineral of choice when dating Himalayan leucogranites, is usually reversely discordant in U–Pb space. This behaviour is interpreted to reflect an initial U–Th disequilibrium caused by the incorporation of excess ^{230}Th during crystallisation, leading to an excess of ^{206}Pb (Schärer 1984). The presence of excess ^{206}Pb results in the $^{206}Pb/^{238}U$ ages for monazite in this study being older than the $^{207}Pb/^{235}U$ and $^{208}Pb/^{232}Th$ ages by as much as 50% (Cottle *et al*. 2009). U–Pb dates can be corrected for the U–Th disequilibrium by estimating the degree of U–Th fractionation between mineral and melt (Schärer 1984; Parrish 1990), but given that the Th–Pb system and the $^{207}Pb/^{235}U$ ages are unaffected by this disequilibrium the $^{207}Pb/^{235}U$ or $^{208}Pb/^{232}Th$ dates are generally taken as the most reliable estimates of the ages of the grains measured.

Most U(–Th)–Pb ages for the melts in the central Himalaya (Fig. 1) are Early–Middle Miocene, ranging from 24–15 Ma (Harrison *et al*. 1995; Hodges *et al*. 1996; Coleman 1998; Searle *et al*. 1997, 1999a, b; Godin *et al*. 2001; Daniel *et al*. 2003; Harris *et al*. 2004; Cottle *et al*. 2009) to 13–12 Ma (Edwards & Harrison 1997; Wu *et al*. 1998; Zhang *et al*. 2004). However, evidence for leucosome melt production during the Oligocene (33–23 Ma) also exists (Coleman 1998; Thimm *et al*. 1999; Godin *et al*. 2001). In the Everest transect the oldest record of *in situ* partial melting occurs in the Namche orthogneiss at ~25–26 Ma (Viskupic & Hodges 2001). Immediately following initial melting, a major phase of pre- to syn-kinematic melt mobilisation occurred between ~22 and 21 Ma (Simpson *et al*. 2000; Viskupic & Hodges 2001; Searle *et al*. 2003; Viskupic *et al*. 2005). The timing of this earliest melt mobilisation is broadly synchronous with emplacement of many of the large granite sheets present at the highest structural level in the Everest region GHS, such as the Everest/Makalu granite (Schärer 1984; Simpson *et al*. 2000). Early foliation parallel granite sheets have U–Pb monazite ages spanning 24–18 Ma (Schärer 1984; Viskupic & Hodges 2001; Searle *et al*. 2003; Viskupic *et al*. 2005; Cottle *et al*. 2009), whereas later sets of undeformed dikes cross-cut ductile fabrics and have U(–Th)–Pb ages of ~18–16 Ma (Hodges *et al*. 1998; Murphy & Harrison 1999; Simpson *et al*. 2000; Viskupic & Hodges 2001; Searle *et al*. 2003; Viskupic *et al*. 2005).

4. Melt reactions

During progressive metamorphism, water-saturated melting may occur if a hydrous fluid phase is present when rocks cross the wet granite solidus. At mid-crustal pressure, appropriate simplified reactions might be:

$$Ms + Qtz + Pl + Kfs + H_2O = Melt$$
$$Ms + Qtz + Pl + H_2O = Sil + Melt$$

Unless there is an external supply of aqueous fluid, however, the amount of melt generated by these vapour- (or fluid-) present processes will be trivial, and significant melt generation will require access to the water locked up in hydrous minerals such as micas or amphiboles. These reactions are referred to as vapour-absent or dehydration melting reactions, and are incongruent melting reactions yielding solid peritectic products. Vapour-absent dehydration melting reactions generally have positive P–T slopes, with the two important consequences that, first, they can be intersected by rocks on a decompression path, and secondly, that in principle the melts generated are able to rise a considerable distance in the crust before reaching their solidus. The first such reaction encountered by a typical

https://doi.org/10.1017/S175569100901617X Published online by Cambridge University Press

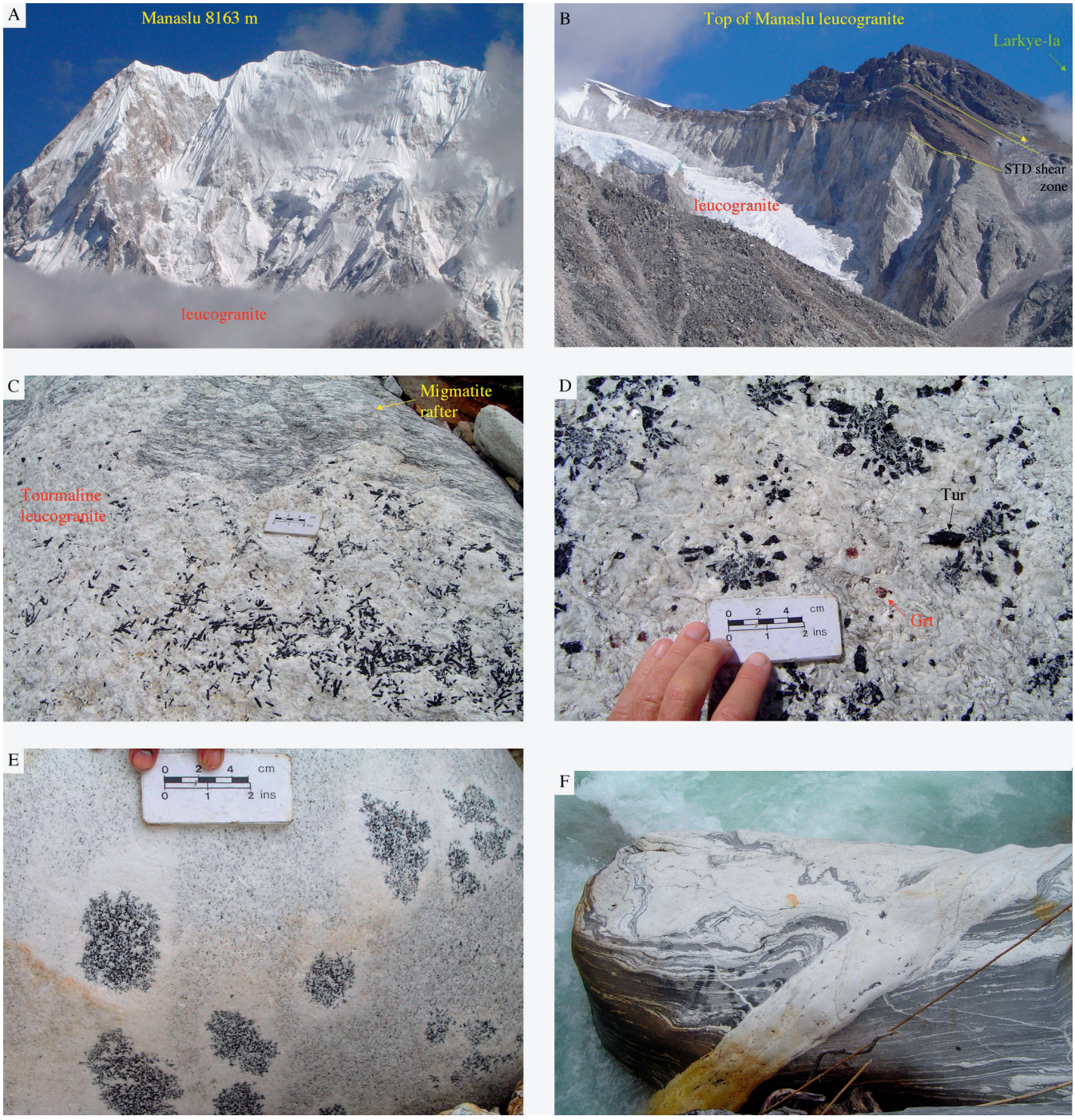

Figure 5 (a) Massive cliffs, approximately 3000 metres high, of pale leucogranite exposed on the south face of Manaslu (8163 m). (b) Upper contact of the Manaslu leucogranite truncated by the north-dipping STD low-angle normal fault; north of the Larkye-la, Nepal–Tibet border. (c) Toumaline leucogranite enclosing rafts of migmatitic gneiss, Bimthang, Manaslu west. (d) Tourmaline+garnet leucogranite, Bimthang, south of Manaslu. (e) Metasomatic 'ghosts' of tourmaline+quartz schorl within leucogranite, Manaslu west. (f) Leucogranite dyke cross-cutting gneissic fabrics, Jangle Karkar, south of Manaslu.

metapelite at mid-crustal depths is likely to be the muscovite dehydration melting reaction:

$$\text{Ms} + \text{Qtz} + \text{Pl} = \text{Kfs} + \text{Als (Sil)} + \text{Melt}$$

Experimental studies in the pressure range 6–10 kbar suggest that this curve is located between about 710°C and 790°C at 8 kbar (Petö 1976; Patiño-Douce & Harris 1998). Its calculated position, in the middle of this range, is shown in Figure 3. The amount of melt generated is typically of the order of ten volume percent, but depends primarily on the amount of muscovite present. Large migmatite terranes represent the *in situ* melt region. During muscovite melting, if the restite and liquid remain in equilibrium, melting will continue until the solid muscovite reactant phase is exhausted.

The biotite dehydration melting reaction:

$$\text{Bt} + \text{Pl} \pm \text{Als (Sil)} + \text{Qtz} = \text{Kfs} \pm \text{Crd} \pm \text{Grt} + \text{Melt}$$

occurs at higher temperature and lower pressure than muscovite melting. Le Breton & Thompson (1988) located the beginning of biotite dehydration melting between 760°C and 800°C at 10 kbar, although significant volumes of melt were not produced until temperatures reached 850°C. Pelitic source rocks will melt at lower temperatures (ca. 750°C; 5 kbar) whereas greywacke source rocks lacking sillimanite require

https://doi.org/10.1017/S175569100901617X Published online by Cambridge University Press

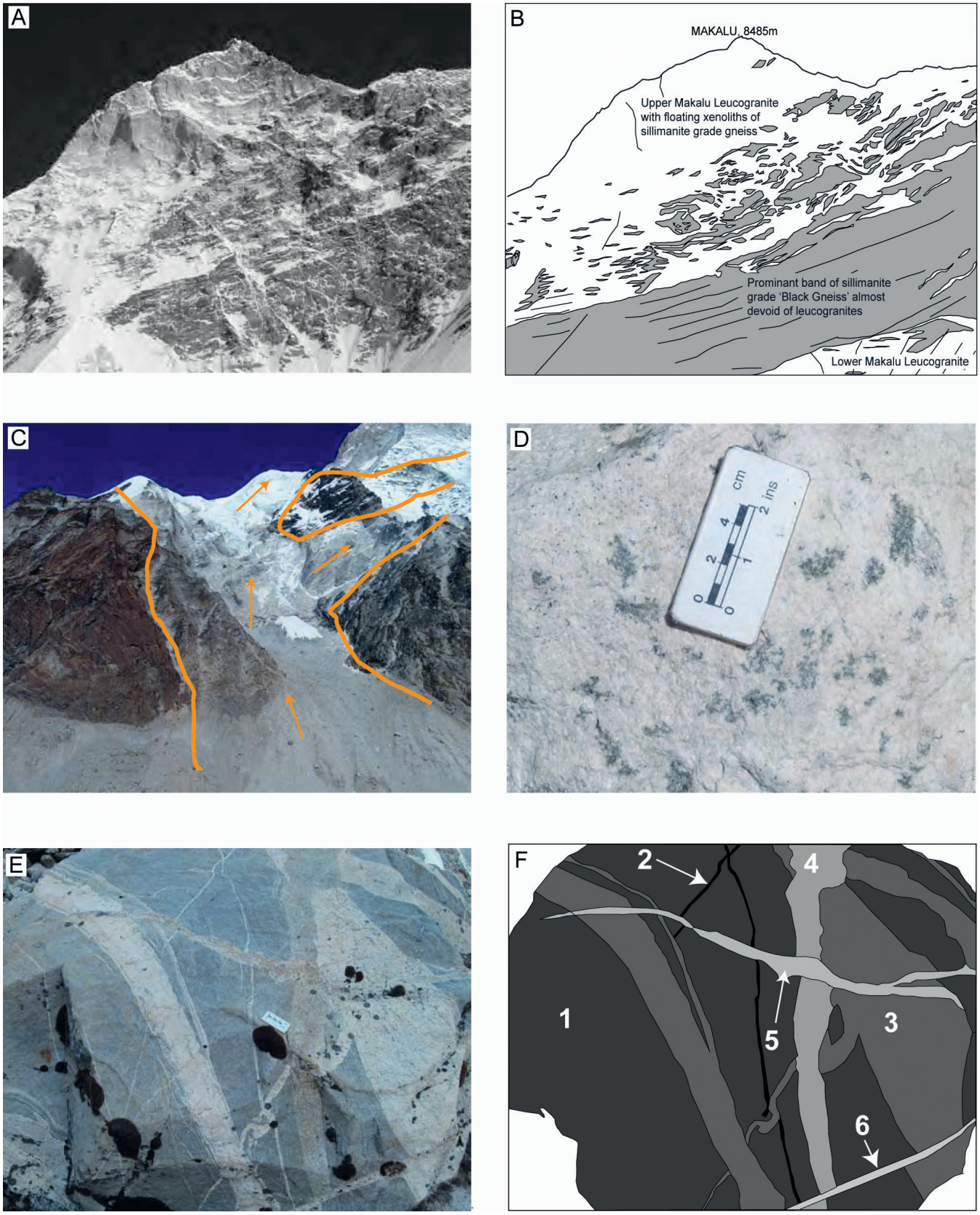

Figure 6 (a), (b) Massive cordierite-bearing leucogranite on the south face of Makalu (8485 m) showing abundant xenoliths along the base of the uppermost large sill. (c) Vertical feeder dyke to the uppermost cordierite leucogranite sill on the south face of Makalu. (d) Large green cordierite crystals enclosed in Makalu leucogranite, Barun glacier, Nepal. (e), (f) Six phases of cross-cutting leucogranite dykes, south face of Makalu, Barun glacier.

higher temperatures of about 825°C at 5 kbar (Vielzeuf & Holloway 1988; Stevens *et al.* 1997). Biotite dehydration melting results in formation of peritectic garnet and/or cordierite in metapelites and peritectic orthopyroxene in metagreywackes. For typical metapelite bulk compositions, cordierite is the stable phase at pressures less than about 5 kbar, whereas garnet is stable at higher pressure.

Himalayan metamorphism records clockwise P–T–t paths with sillimanite grade overprinting earlier kyanite grade conditions. Harris & Massey (1994) concluded that most

https://doi.org/10.1017/S175569100901617X Published online by Cambridge University Press

Himalayan granites were decompression melts formed on the exhumation part of the P–T path in the sillimanite field. However, the uncommon presence of kyanite-bearing migmatites, e.g. in the Marsyandi valley, Nepal (Coleman 1998), in Bhutan (Daniel *et al.* 2003) and in Sikkim, is evidence that melting probably started earlier (23–16 Ma from garnet Sm–Nd ages in Harris *et al.* 2004), and at higher pressure (8–12 kbar) in some parts of the Himalaya.

P–T phase relations and trace element modelling suggest that most Himalayan leucogranites formed by vapour-absent incongruent melting of muscovite in the temperature range 650–750°C at pressures between 9 and 4 kbar (Scaillet *et al.* 1990, 1996; Harris & Massey 1994; Searle *et al.* 1999b; Prince *et al.* 2001). A flux of aqueous fluid into the melting zone will augment the volume of granitic melt formed. There is geochemical evidence that melting was not typically an equilibrium process (Harris & Inger 1992), and that extracted melt entrained a proportion of restitic material. Incomplete mixing between different melt batches resulted in isotopic heterogeneity in crystallised leucogranite bodies (e.g. Deniel *et al.* 1987; Scaillet *et al.* 1996).

These crustal melt reactions require no heat or chemical input from the mantle. The achievement of high temperatures in the mid-crust would, however, be assisted by high internal heat production in the source region. In a ductile deforming channel such as the Early Miocene GHS, internal heat production could include both radiogenic and strain heating. In the following sections it is suggested that this is the case.

5. Source rocks

Himalayan leucogranites are strongly peraluminous, characterised by the presence of muscovite and tourmaline, with biotite and garnet also present in lesser amounts. Major element compositions are fairly homogeneous, but trace elements are highly variable and depend on the nature of the source. Sr, Nd and Pb isotopes are all indicative of a metasedimentary source (Deniel *et al.* 1987; Harris *et al.* 1995, Guillot & LeFort 1995). $^{87}Sr/^{86}Sr$ ratios of leucogranites are very high (0·74–0·79) and heterogeneous, suggesting a 100% crustal protolith. Harris & Massey (1994) made a detailed Sr isotope study of the Langtang leucogranites and concluded that the protolith was not the sillimanite migmatites into which the melts have been emplaced, but rather the kyanite-bearing meta-pelites structurally lower down the GHS section. They further implied that the granites were not *in situ* melts but had migrated some distance (>10 km) from their source. However, in most Himalayan profiles mapped by the present authors it is possible to physically trace the migmatite leucosomes coalescing into giant foliation-parallel sill networks, which feed larger plutons (e.g. Searle *et al.* 1997, 1999b). It is perfectly possible that the leucogranite bodies were tapping different migmatites at depth rather than ones immediately adjacent (Harris & Massey 1994) but the heterogeneous Sr isotopes probably reflect a wide range of protoliths with each batch of melt produced.

The leucogranite sill complexes are almost always within the sillimanite grade gneisses and melt migration was more horizontal, not vertical. The larger plutons are not actually intrusive into higher structural levels, but are more like subhorizontal ballooning sills (e.g. Nuptse leucogranite; Searle *et al.* 2003, Searle 2003, 2007). This is the case in Zanskar (e.g. Noble & Searle 1995), Shivling, Garhwal (Searle *et al.* 1993, 1999b), Manaslu (Searle & Godin 2003), Shisha Pangma (Searle *et al.* 1997), and the Everest region (Searle 1999a, b, 2003; Searle *et al.* 2003, 2006; Jessup *et al.* 2008).

Isotopic signatures can be used to determine the nature of granite protoliths, provided that the liquid is in isotopic equilibrium with the source. Trace element modelling of partial melting is only useful if equilibrium between the melt and the solid phases has been achieved (Harris & Inger 1992; Harris *et al.* 1995). Himalayan leucogranites are, however, rarely in isotopic equilibrium as a result of complex sedimentary protoliths and multiple batch melting (Deniel *et al.* 1987). Guillot & LeFort (1995) proposed a bimodal origin of Himalayan leucogranites with two-mica leucogranites ($^{87}Sr–^{86}Sr$ ratio <0·752) derived from a meta-greywacke source and tourmaline leucogranites ($^{87}Sr–^{86}Sr$ ratio >0·752) derived from a metapelitic source. However, in the field there is a complete range of granite composition with variable amounts of tourmaline, muscovite, biotite and garnet. It seems more likely that progressive batch melting tapped different source rocks ranging from black shales to meta-greywackes within the NeoProterozoic Haimanta Formation. Cambro-Ordovician augen gneisses (Formation 3; LeFort 1975, 1981) also commonly show *in situ* melt textures with tourmaline ± garnet bearing leucosomes.

6. Heat source for crustal melting

It has become increasingly clear that peak sillimanite grade metamorphism, crustal melting and ductile shear along the MCT along the base of the GHS and ductile shear along the STD at the top of the GHS were synchronous, and these metamorphic, magmatic and structural processes must be genetically linked. The greatest problem has been to explain why peak temperatures and granite melt generation in thickened Himalayan crust were at a relatively shallow depth (15–20 km depth; 4–6 kbar), and why melting does not occur at greater depths. P–T–t data across the GHS along the Everest profile show that high temperatures (>620°C) were maintained for ca. 15 million years (from 32 to 17 Ma) along the top of the GHS and that approximately 45–50 km width (20 km structural thickness) of the GHS was approximately isothermal in the sillimanite grade (Searle *et al.* 2003, 2006; Jessup *et al.* 2006, 2008). This shallow heating requires an unusually steep geothermal gradient, and crustal thickening alone cannot account for the thermal profile. Restoration of the GHS shows that the source for granite melts was the Neo-Proterozoic Haimanta–Cheka Formation. A combination of high internal radiogenic heat production from the melt source rocks and thermal relaxation after crustal thickening is proposed. Average heat production in the migmatites is a factor of two more than heat production in the schists (Harris & Massey 1994). Shear heating along the MCT (England *et al.* 1992; Harrison *et al.* 1998) cannot explain the heat distribution in the GHS because maximum temperatures are a long way up-section from the MCT. No granite melts are present along the exposed MCT anywhere along the Himalaya. No mantle heat input is present, so the only possible extra heat source for restricted shallow-level melting is internal heat production by highly radioactive sedimentary source rocks. Gariepy *et al.* (1985) noted that Himalayan granites have highly radiogenic Pb isotopic compositions which imply sources enriched in U and Th. Uranium concentrations from Himalayan granites are some of the highest found anywhere in granitic rocks (Pinet & Jaupart 1987).

7. Melt segregation – migmatites

The core of the GHS shows a vast migmatite terrane that stretches from the ductile shear zone along the STD at the top to the region above the zone of inverted metamorphic

https://doi.org/10.1017/S175569100901617X Published online by Cambridge University Press

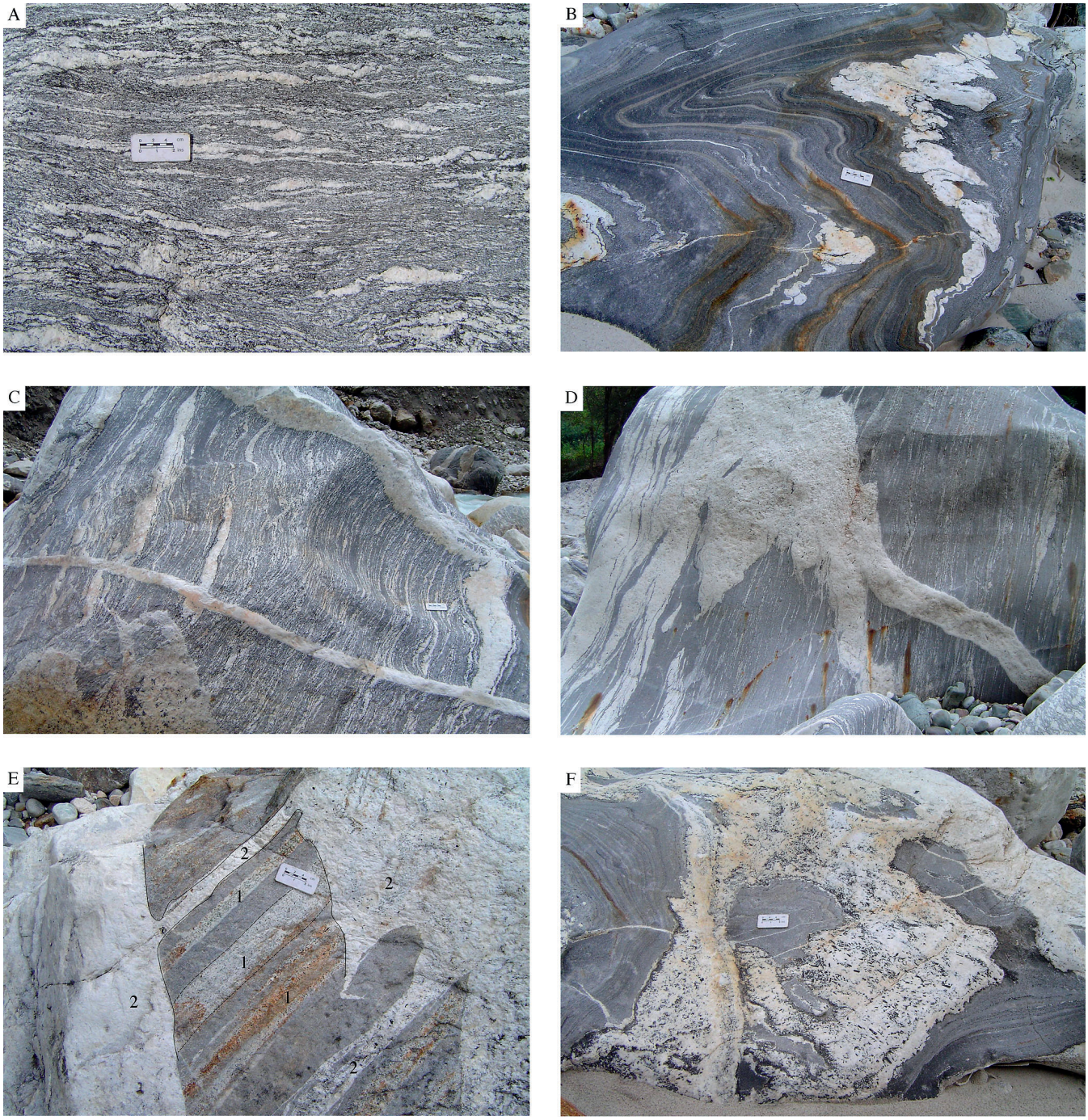

Figure 7 (a) Typical migmatite textures showing stromatic migmatite with melts generated along the foliation planes, south of Manaslu in the Marsyandi valley, Nepal. (b) Early leucogranites boudinaged in the foliation plane and subsequently folded, south of Manaslu, Nepal. (c) Melt extraction textures where melt is channelled out of leucosome into dykes that mobilise and cross-cut the migmatite fabric, south of Manaslu, Nepal. (d) Melt mobilisation from leucosome to channelled flow along dykes, south of Manaslu. (e) Early layered leucogranite sills (1) in gneisses, cut by late granite melts mobilised into sill-dyke networks (2), south of Manaslu, Nepal. (f) Late tourmaline leucogranite melts breaking up host gneisses into xenoliths, south of Manaslu, Marysandi valley, Nepal.

isograds along the MCT at the base. The zone of partial melting above the sillimanite–K-feldspar isograd can reach a maximum structural thickness of 15–20 km along the Zanskar profile in the western Himalaya (Searle & Rex 1989; Searle *et al.* 1992, 1999a, b), and 20 km along the Everest profile in Nepal (Searle *et al.* 2003, 2006; Jessup *et al.* 2006) and the Kangchenjunga profile in Sikkim (Searle & Szulc 2005). Although the protoliths differ (from Proterozoic in the south to Cambro-Ordovician in the north), metamorphic grade, P–T conditions and degrees of partial melting are similar across the GHS. *In situ* crustal melting forming migmatites is common in GHS quartzo-feldspathic gneisses, pelitic gneisses and K-feldspar augen gneisses. From field evidence it seems likely that all these lithologies constituted source rocks for granite melts.

Melt extraction pathways can be mapped out using leucosome networks. Layered stromatic migmatites are the most common textures, with melt segregations flattened in the foliation plane (Fig. 7a), similar to compaction bands (e.g. Brown 2007). K-feldspar augen gneisses commonly show *in situ* melting, for example in the Namche orthogneiss (Viskupic & Hodges 2001; Searle *et al.* 2003). Kinematic

https://doi.org/10.1017/S175569100901617X Published online by Cambridge University Press

indicators (rotated K-feldspar augen, C–S fabrics, etc.) and quantitative strain data from the Everest profile show that although south-directed simple shear is dominant across the GHS, a significant component of pure shear is apparent (Law *et al.* 2004; Jessup *et al.* 2006). This general shear is compatible with flow parallel to the extension direction in horizontal sheeted leucogranite sills. U–Pb dating of monazite shows that migmatite leucosomes have Early Miocene ages, similar to the higher level leucogranites (Noble & Searle 1995; Walker *et al.* 1999; Dezes *et al.* 1999), supporting a genetic relationship between migmatite and granite, despite the difference in Sr and O isotopes (Harris & Massey 1994).

Pervasive melt migration can initially occur by porous melt flow through hot, viscous crust (Weinberg & Searle 1999). This is like an intermediate stage between a migmatite terrane and a sheeted sill complex. Cross-cutting relationships show batch melting of leucogranite with early formed granites folded in with the schistosity (Fig. 7b). Early leucogranite sills commonly show boudinage fabrics, indicating extension at right angles to the flattening direction. Leucosomes are randomly distributed in the core of the GHS where exposed, but begin to coalesce into discrete veins and melt channels that tend to follow planes of anisotropy. As soon as leucosome *in situ* melts become interconnected, the melt extraction pathway is formed and the melt may start to flow (Fig. 7c, d). High-temperature igneous textures show that melt extracted from the migmatite feeds dykes may cross-cut the same migmatite fabric (Fig. 7e). Thus very short time intervals between melt extraction, dyking and crystallisation are involved in each batch of melt. Later foliation-parallel sheeted sill complexes feed magma, generated from the migmatite zone, horizontally along the foliation planes of anisotropy. Later dykes cross-cut the migmatite fabric and contain floating xenoliths of migmatitic gneiss within (Fig. 7f). Melt flows down pressure gradients by the easiest path, feeding magma to higher level sills. In the Himalaya these flow pathways gently up-dip from north to south along north-dipping foliation planes.

8. Melt transport; granite emplacement mechanisms

Several Himalayan leucogranites have been mapped out in 3-D and studied in detail. These include the Shivling–Bhagirathi granites in north India (Scaillet *et al.* 1990, 1995; Searle *et al.* 1993), the Manaslu leucogranite in west Nepal (Guillot *et al.* 1993, 1995; Searle & Godin 2003), the Shisha Pangma leucogranite in south Tibet (Searle *et al.* 1997) and the Everest–Makalu leucogranites in east Nepal–south Tibet (Searle 1999a, b, 2003; Searle *et al.* 2003, 2006; Jessup *et al.* 2006). Spectacular sheeted sill networks of leucogranite melts can be seen in many 3-D cliff sections along the Himalaya. Sills propagate by hydraulic fracturing, forcing cracks apart to accommodate magma injected from the migmatite zone. Composite intrusions show that multiple batches of magma are injected into the same zone. Occasional dykes connect sills, enabling magma to be channelled up structural section. Magma batches may be separated by short time intervals. Some outcrops show foliation-parallel sills concordant with the metamorphic fabric in the host sillimanite gneiss, which feed magma into a dyke that clearly crosscuts the same metamorphic fabric.

In the Himalaya there is almost no evidence of diapiric ascent of granite magma. Despite some earlier studies describing diapiric intrusions of the Manaslu leucogranite up across the STD into Tethyan sediments (LeFort 1975, 1981; Colchen *et al.* 1986; Harrison *et al.* 1999), subsequent work has shown that the granite was intrusive into high-grade marbles, augen gneiss and pelite of the GHS and that the STD wraps around the top of the leucogranite (Searle & Godin 2003). All Himalayan leucogranites are within the GHS, beneath the STD passive roof fault. In the deeper structural levels magma flow is almost entirely sub-horizontal along foliation-parallel sill complexes. At higher structural levels the sills amalgamate into larger sills and, as they approach the surface, they balloon up into inflated sills. This ballooning sill structure is typified by the Nuptse sill in the Everest region (Searle 1999a, b, 2003) and by the Shisha Pangma leucogranite in south Tibet (Searle *et al.* 1997). Even the largest Himalayan leucogranites such as the Manaslu (ca. 5 km thick) leucogranite are tabular sill-like bodies dipping gently north and truncated along the top by the STD ductile shear zone and low-angle normal fault (Searle & Godin 2003; Fig. 5b). Similarly, the Kangchenjunga leucogranite is a series of composite sills totalling approximately 12–14 km structural thickness (Searle & Szulc 2005), dipping gently north and truncated by the STD along the top.

In addition to field observations, the petrological and isotopic heterogeneity of leucogranites, and a thin upper thermal aureole, has been used as evidence for episodic emplacement of magmas to form larger leucogranite bodies. Thermal modelling of this emplacement (Annen *et al.* 2006) implies a 20–60 ka repeat time for the emplacement of 20–60 m-thick sills which form the larger 5 km-thick Himalayan leucogranite bodies (e.g. Manaslu, Fig. 5). To provide such a volume of melt, a highly fertile source must be heated for a prolonged time, producing low viscosity ($10^{4\cdot5}$PaS) magma that is emplaced via shear assisted melt extraction (Scaillet & Searle 2006).

9. Channel Flow model

The Himalayan Channel Flow model (Fig. 8) describes a protracted flow of a weak, viscous, partially molten layer of middle crust between relatively rigid, but still deformable bounding upper and lower crust slabs (e.g. Beaumont *et al.* 2001, 2004; Grujic *et al.* 2002; Godin *et al.* 2006; Grujic 2006). Ductile extrusion of high-grade metamorphic rocks, and leucogranite melts between a coeval normal sense shear zone above (STD) and a thrust-sense shear zone below (MCT) allowed southward extrusion of the GHS. The resultant geometry of the metamorphic isograds shows an inverted and condensed P–T profile above the Main Central Thrust along the base of the extruding slab (Searle & Rex 1989; Searle *et al.* 2008) and a right-way-up P–T profile beneath the South Tibetan Detachment along the top of the extruding slab (Searle *et al.* 2003, 2006; Jessup *et al.* 2006). Extrusion was driven ultimately by the crustal thickness and topographic variation between the Tibetan plateau hinterland (70–80 km thick crust; ca. 5 km elevation) and the Indian foreland (35–40 km thick crust, 0–1 km elevation).

Numerous geological studies across the GHS have shown that almost all the data supports the Channel Flow model for the GHS during the Early Miocene. These data include P–T profiles (e.g. Searle *et al.* 2003, 2006; Jessup *et al.* 2006), 3-D distribution of partial melts and granites in the middle crust (e.g. Searle 1999a, b; Searle *et al.* 1999a, b, 2006; Searle & Szulc 2005), and quantitative data on strain, deformation temperatures and vorticity of flow (e.g. Law *et al.* 2004; Jessup *et al.* 2006). Beaumont *et al.* (2001) used a thermal-mechanical numerical model to show that channel flow and ductile extrusion were dynamically linked to the effects of surface erosion focused along the Greater Himalaya at the extrusion front. As pointed out by Klemperer (2006) this model is consistent with

https://doi.org/10.1017/S175569100901617X Published online by Cambridge University Press

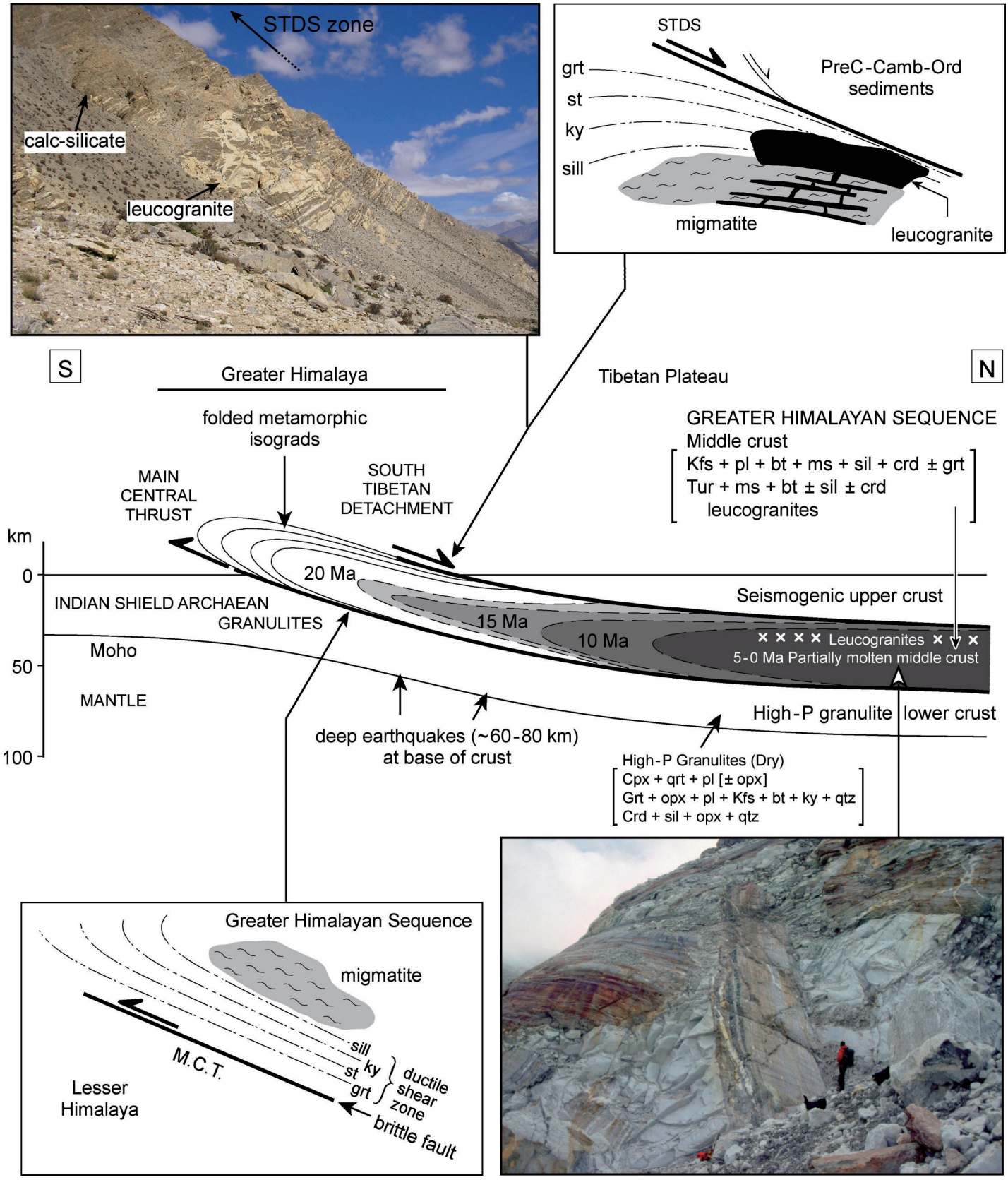

Figure 8 Himalayan channel flow model (after Searle *et al.* 2006; Cottle *et al.* 2009), a model that satisfies all geological and geophysical requirements in the Greater Himalaya. Inset top left shows the STD profile along Dzakaa chu, north of Everest, South Tibet. Inset bottom right shows the central part of the channel in the Kangshung valley east of Everest, south Tibet. Giant blocks or rafters of gneisses with early leucogranite sills are completely enclosed in Miocene leucogranite.

all the geological data . . . 'inevitably, since the model was designed *a posteriori* to fit the observations'.

Searle *et al.* (1988) and Searle & Rex (1989) first proposed that inverted, condensed metamorphic isograds from kyanite to biotite grade along the MCT ductile shear zone along the base of the GHS channel were linked to the right-way-up isograds along the footwall of the STD along the top of the GHS. Kinematic indicators and strain requires the GHS to be

https://doi.org/10.1017/S175569100901617X Published online by Cambridge University Press

extruding south relative to the stable seismogenic upper crust above (Tethyan Himalaya), and the subducting Indian shield and Lesser Himalayan cover rocks beneath. Later models based on the Bhutan Himalaya (Grujic *et al.* 1996, 2002) included the folded isograds in their wedge extrusion or layer extrusion models. Deep crustal seismic profiling now reveals that the partially molten mid-crustal layer imaged beneath southern Tibet can match the geologically constrained cross-sections across the GHS in Nepal (Nelson *et al.* 1996; Searle *et al.* 2003, 2006).

Extensive geophysical measurements in Tibet also imply that temperatures and rheologies require some form of crustal flow. Seismic velocities beneath southern Tibet are so low that the crust has to be fluid-rich, and predicted temperatures are so high that these fluids are likely to be partial melts. Low elastic thickness, low topographic relief and shallow cut-off of crustal seismicity all show that fluids weaken the middle crust (Klemperer 2006). The 'bright spots' as imaged by magneto-telluric studies beneath the Lhasa block (Wei *et al.* 2001; Unsworth *et al.* 2005), are at the same structural depth as the depth of formation of Himalayan leucogranites (Searle *et al.* 2003, 2006; Galliard *et al.* 2004) and in a similar down-dip structural position in the middle crust. Unlike the middle crust, the lower crust beneath the Himalaya and southern Tibet is relatively rigid and not melting, suggesting that it is composed of dry granulite facies metamorphic rocks of the underthrust lower Indian crust. Because crustal thickness reaches 75–80 km beneath southern Tibet (Nelson *et al.* 1996) or even up to 90 km beneath the Karakoram and western Tibet (Rai *et al.* 2006), the lower crust beneath these regions must be in high-pressure granulite (dry) or eclogite (wet) metamorphic facies today (Searle *et al.* 2003, 2006). Brown & Solar (1998) and Brown (2006, 2007) proposed that melt loss in the middle crust might leave a dry granulite residue behind in the lower crust. The lower crust in the Himalaya is inherited Precambrian granulite facies rocks, which are anhydrous and strong and can also explain the deep crustal seismicity beneath southern Tibet (Priestley *et al.* 2008).

10. Conclusions

The unique three-dimensional exposures around Himalayan leucogranites allow a comprehensive view of their internal and external structure to be mapped out. Extensive study of fabrics in the host gneisses, migmatites, leucogranite sills, dykes and larger bodies combined with detailed U–(Th)–Pb dating of peak metamorphic, migmatite leucosome and granite melting have allowed the fourth dimension, time, to be incorporated into models of melt generation and emplacement. Along the 2200 km length of the Himalaya, the larger leucogranite bodies always occur at similar structural horizons within the upper part of the GHS, beneath the STD low-angle normal fault. The STD forms a passive roof (stretching) fault (Searle *et al.* 2003; Law *et al.* 2004), beneath which channel flow and ductile extrusion of the GHS middle crust occurred.

Himalayan crustal melting occurred along the upper part of the middle crust (4–6 kbar; 15–20 km depth), but not in the lower crust. Sr, Nd and O isotopes indicate pure crustal melting with no input from the mantle. Melts were sourced from fertile muscovite-bearing pelites and quartzo-feldspathic gneisses of the Neo-Proterozoic Haimanta–Cheka Formations. The primary heat source was probably from high internal heat production rates within the Proterozoic source rocks in the middle crust. A vast *in situ* migmatite terrane generated melts from the melting of a heterogeneous variety of protolith rocks. Interconnected leucosome melts aggregated to force magma into layer-parallel sills and a few cross-cutting dykes. Early Miocene leucogranites (24–17 Ma) are largely concordant with the foliation, whereas later ones (16–12 Ma) may cross-cut the ductile fabrics. All leucogranites are cut by the uppermost brittle low-angle normal fault, the Qomolangma detachment.

Field observations, structural sections and geophysical evidence all provide support for the Channel Flow model, a description of the evolution of the Himalayan–south Tibetan crust during the Miocene. The Himalayan channel flow model is restricted both in time (Early–Middle Miocene) and space (Himalayan–south Tibet middle crust). It is not applicable to the earlier, Eocene subduction-related UHP coesite eclogite metamorphism, or to the Oligocene HP kyanite metamorphism. Whether channel flow is active today in the middle crust of southernmost Tibet–northernmost Himalaya is still open to debate (Nelson *et al.* 1996; Hodges 2000; Searle *et al.* 2006). The present model (Fig. 8) shows that the Greater Himalaya may represent the Miocene carapace of an actively extruding mid-crustal channel operating at depth beneath southern Tibet today.

11. Acknowledgements

This work was carried out using NERC grant NER/K/S/2000/00951 to MPS and PhD grants to JMC (New Zealand TEC scholarship) and MJS (NERC). We are grateful to Randall Parrish, Steve Noble, Bruno Scaillet, Laurent Godin, Rick Law, Micah Jessup and the late Doug Nelson for discussions. We also thank Peter Treloar and Alan Whittington for detailed and insightful reviews, and Alex Kisters for editorial and scientific comments.

12. References

Annen, C., Scaillet, B. & Sparks, R. S. J. 2006. Thermal constraints on the emplacement rate of a large intrusive complex: The Manaslu leucogranite, Nepal Himalaya. *Journal of Petrology* **47**, 71–95.

Beaumont, C., Jamieson, R. A., Nguyen, M. H. & Lee, B. 2001. Himalayan tectonics explained by extrusion of a low-viscosity crustal channel coupled to focused surface denudation. *Nature* **414**, 738–42.

Beaumont, C., Jamieson, R. A., Nguyen, M. H. & Medvedev, S. 2004. Crustal channel flows: 1. Numerical models with applications to the tectonics of the Himalayan–Tibetan orogen. *Journal of Geophysical Research – Solid Earth* **109**, B06406.

Booth, A. L., Zeitler, P. K., Kidd, W. S. F., Wooden, J., Liu, Y. P., Idleman, B., Hren, M. & Chamberlain, C. P. 2004. U–Pb zircon constraints on the tectonic evolution of southeastern Tibet, Namche Barwa area. *American Journal of Science* **304**, 889–929.

Bowring, S. A., Searle, M. P., Waters, D. J., Hodges, K. V., Schmitz, M. & Crowley, J. 2004. ID–TIMS geochronology of ca. 1 Ma leucogranites from the core of Nanga Parbat. *American Geophysical Union Fall Meeting San Francisco*, V22E-08.

Brown, M. 2006. Melt extraction from the lower continental crust of orogens: the field evidence. *In* Brown, M. & Rushmer, T. (eds) *Evolution and Differentiation of Continental Crust*, 332–84. Cambridge: Cambridge University Press.

Brown, M. 2007. Crustal melting and melt extraction, ascent and emplacement in orogens: mechanisms and consequences. *Journal of the Geological Society London* **164**, 709–30.

Brown, M. & Solar, G. S. 1998. Shear zone systems and melts: feedback relations and self-organization in orogenic belts. *Journal of Structural Geology* **20**, 211–27.

Burg, J. P. 1983. *Geological Map of South Tibet.* Beijing: Ministry of Geology.

Butler, R. W. H., Harris, N. B. W. & Whittington, A. G. 1997. Interactions between deformation, magmatism and hydrothermal activity during active crustal thickening: a field example from Nanga Parbat, Pakistan Himalayas. *Mineralogical Magazine* **61**, 37–51.

Colchen, M., LeFort, P. & Pecher, A. 1986. *Annapurna–Manaslu–Ganesh Himal. Carte geologique au 1:200 000 scale*. Paris: CNRS. 136 pp.

Coleman, M. E. 1998. U–Pb constraints on Oligocene–Miocene deformation and anatexis within the central Himalaya, Marsyandi Valley, Nepal. *American Journal of Science* **298**, 553–71.

https://doi.org/10.1017/S175569100901617X Published online by Cambridge University Press

Copeland, P., Parrish, R. R. & Harrison, T. M. 1988. Identification of inherited radiogenic Pb in monazite and its implications for U–Pb systematics. *Nature* **333**, 760–3.

Cottle, J. M., Jessup, M. J., Newell, D. L., Searle, M. P., Law, R. D. & Horstwood, M. S. A. 2007. Structural insight into the ductile evolution of an orogen-scale detachment: the South Tibetan Detachment System, Dzakaa Chu section, Eastern Himalaya. *Journal of Structural Geology* **29**, 1781–97. doi:10.1016/j.jsg.2007.08.007.

Cottle, J. M., Searle, M. P., Horstwood, M. S. A. & Waters, D. J. 2009. Timing of mid-crustal metamorphism, melting and deformation in the Mount Everest region of Southern Tibet revealed by U(–Th)–Pb geochronology. *Journal of Geology* **117**(6), 643–64. doi: 10.1086/605994

Crowley, J. L., Bowring, S. A. & Searle, M. P. 2005. U–Th–Pb systematics of monazite, xenotime, and zircon from Pleistocene leucogranites at Nanga Parbat (Pakistan Himalaya). *Geochimica et Cosmochimica Acta* **69**, 8.

Crowley, J. L., Waters, D. J., Searle, M. P. & Bowring, S. A. 2009. Pleistocene melting and rapid exhumation of the Nanga Parbat massif, Pakistan: Age and P–T conditions of accessory mineral growth in migmatite and leucosome. *Earth and Planetary Science Letters* **288**, 408–20. doi: 10.1016/j.epsl.2009.09.044

Daniel, C. G., Hollister, L. S., Parrish, R. R. & Grujic, D. 2003. Exhumation of the Main Central Thrust from lower crustal depths, Eastern Bhutan Himalaya. *Journal of Metamorphic Geology* **21**, 317–34.

Deniel, C., Vidal, P., Fernandez, A., Le Fort, P. & Peucat, J. J. 1987. Isotopic study of the Manaslu granite (Himalaya, Nepal); inference on the age and source of Himalayan leucogranites. *Contributions to Mineralogy and Petrology* **96**, 78–92.

Dezes, P., Vannay, J.-C., Steck, A., Bussy, F. & Cosca, M. 1999. Synorogenic extension: Quantitative constraints on the age and displacement of the Zanskar shear zone (northwest Himalaya). *Geological Society of America Bulletin* **111**, 364–74.

Edwards, M. A. & Harrison, T. M. 1997. When did the roof collapse? Late Miocene north–south extension in the high Himalaya revealed by Th–Pb monazite dating of the Khula Kangri Granite. *Geology* **25**, 543–6.

England, P., LeFort, P., Molnar, P. & Pêcher, A. 1992. Heat sources for Tertiary metamorphism and anatexis in the Annapurna–Manaslu region central Nepal. *Journal of Geophysical Research* **97**, 2107–28.

Gaillard, F., Scaillet, B. & Pichavant, M. 2004. Evidence for present-day leucogranite pluton growth in Tibet. *Geology* **32**, 801–4.

Gariepy, C., Allegre, C. & Xu, R. H. 1985. Pb-isotope geochemistry of granitoids from the Himalaya–Tibet collision zone: implications for crustal evolution. *Earth and Planetary Science Letters* **74**, 220–34.

Godin, L., Parrish, R. R., Brown, R. L. & Hodges, K. V. 2001. Crustal thickening leading to exhumation of the Himalayan metamorphic core of central Nepal; insight from U–Pb geochronology and $^{40}Ar/^{39}Ar$ thermochronology. *Tectonics* **20**, 729–47.

Godin, L., Grujic, D., Law R. D. & Searle, M. P. 2006. Channel flow, ductile extrusion and exhumation in continental collision zones: an introduction. *In* Law, R. D., Searle, M. P. & Godin, L. (eds) *Channel Flow, Ductile Extrusion and Exhumation in Continental Collision Zones. Geological Society, London, Special Publications* **268**, 1–23.

Grujic, D. 2006. Channel Flow and continental collision tectonics. *In* Law, R. D., Searle, M. P. & Godin, L. (eds) *Channel Flow, Ductile Extrusion and Exhumation in Continental Collision Zones. Geological Society, London, Special Publications* **268**, 25–37.

Grujic, D., Casey, M., Davidson, C., Hollister, L. S., Kundig, R., Pavlis, T. & Schmid, S. 1996. Ductile extrusion of the Higher Himalayan crystalline in Bhutan: Evidence from quartz microfabrics. *Tectonophysics* **260**, 21–43.

Grujic, D., Hollister, L. S. & Parrish, R. R. 2002. Himalayan metamorphic sequence as an orogenic channel: insight from Bhutan. *Earth and Planetary Science Letters* **198**, 177–91.

Guillot, S., Pêcher, A., Rochette, P. & LeFort, P. 1993. The emplacement of the Manaslu granite of Central Nepal: field and magnetic susceptibility constraints. *In* Treloar, P. J. & Searle, M. P. (eds) *Himalayan Tectonics. Geological Society, London, Special Publications* **74**, 413–28.

Guillot, S., LeFort, P., Pêcher, A., Barman, M. R. & Aprahamian, J. 1995. Contact metamorphism and depth of emplacement of the Manaslu granite (central Nepal): implications for Himalayan orogenesis. *Tectonophysics* **241**, 99–119.

Guillot, S. & LeFort, P. 1995. Geochemical constraints on the bimodal origin of High Himalayan leucogranites. *Lithos* **35**, 221–34.

Harris, N. B. W., Ayres, M. & Massey, J. 1994. Geochemistry of granitic melts produced during the incongruent melting of muscovite; implications for the extraction of Himalayan leucogranite magmas. *Journal of Geophysical Research B Solid Earth and Planets* **100**, 15767–77.

Harris, N. B. W., Ayres, M. W. & Massey, J. 1995. Geochemistry of granitic melts produced during the incongruent melting of muscovite: implications for the extraction of Himalayan leucogranite magmas. *Journal of Geophysical Research* **100**, 15767–77.

Harris, N. B. W., Caddick, M., Kosler, J., Goswami, S., Vance, D. & Tindle, A. G. 2004. The pressure–temperature–time path of migmatites from the Sikkim Himalaya. *Journal of Metamorphic Geology* **22**, 249–64.

Harris, N. B. W. & Inger, S. 1992. Trace-Element Modeling of Pelite-Derived Granites. *Contributions to Mineralogy and Petrology* **110**, 46–56.

Harris, N. B. W. & Massey, J. A. 1994. Decompression and anatexis of Himalayan metapelites. *Tectonics* **13**, 1537–46.

Harrison, T. M., McKeegan, K. D. & Le Fort, P. 1995. Detection of inherited monazite in the Manaslu leucogranite by $^{208}Pb/^{232}Th$ ion microprobe dating; crystallization age and tectonic implications. *Earth and Planetary Science Letters* **133**, 271–82.

Harrison, T. M., Grove, M., Lovera, O. M. & Catlos, E. J. 1998. A model for the origin of Himalayan anatexis and inverted metamorphism. *Journal of Geophysical Research* **103**, 27017–32.

Harrison, T. M., Grove, M., McKeegan, K. D., Coath, C. D., Lovera, O. M. & Le Fort, P. 1999. Origin and episodic emplacement of the Manaslu intrusive complex, central Himalaya. *Journal of Petrology* **40**, 3–19.

Hauck, M. L., Nelson, K. D., Brown, L. D., Zhao, W. J. & Ross, A. R. 1998. Crustal structure of the Himalayan orogen at similar to 90 degrees east longitude from Project INDEPTH deep reflection profiles. *Tectonics* **17**, 481–500.

Hodges, K. V. 2000. Tectonics of the Himalaya and southern Tibet from two perspectives. *Geological Society of America Bulletin* **112**, 324–50.

Hodges, K. V., Parrish, R. R. & Searle, M. P. 1996. Tectonic evolution of the central Annapurna Range, Nepalese Himalayas. *Tectonics* **15**, 1264–91.

Hodges, K. V., Bowring, S. A., Davidek, K. L., Hawkins, D. P. & Krol, M. A. 1998. Evidence for rapid displacement on Himalayan normal faults and the importance of tectonic denudation in the evolution of mountain ranges. *Geology* **26**, 483–6.

Hubbard, M. S. 1989. Thermobarometric constraints on the thermal history of the Main Central Thrust Zone and Tibetan Slab, eastern Nepal Himalaya. *Journal of Metamorphic Geology* **7**, 19–30.

Jackson, J., McKenzie, D., Priestley, K. & Emmerson, B. 2008. New views on the structure and rheology of the lithosphere. *Journal of the Geological Society, London* **165**, 453–65.

Jamieson, R. A., Beaumont, C., Medvedev, S. & Nguyen, M. H. 2004. Crustal channel flows: 2. Numerical models with implications for metamorphism in the Himalayan–Tibetan orogen. *Journal of Geophysical Research – Solid Earth* **109**, B06407.

Jessup, M. J., Law R. D., Searle, M. P. & Hubbard, M. S. 2006. Structural evolution and vorticity of flow during extrusion and exhumation of the Greater Himalayan Slab, Mount Everest Massif, Tibet/Nepal; implications for orogen-scale flow partitioning. *In* Law, R. D., Searle, M. P. & Godin, L. (eds) *Channel Flow, Ductile Extrusion and Exhumation in Continental Collision Zones. Geological Society, London, Special Publications* **268**, 379–413.

Jessup, M. J., Cottle, J. M., Searle, M. P., Law, R. D., Newell, D. L., Tracy, R. J. & Waters. D. J. 2008. P–T–t–D paths of Everest Series schist, Nepal. *Journal of Metamorphic Geology* **26**, 717–39. doi: 10.1111/j.1525-1314.2008.00784.x

Klemperer, S. L. 2006. Crustal flow in Tibet; geophysical evidence for the physical state of Tibetan lithosphere, and inferred patterns of active flow. *In* Law, R. D., Searle, M. P. & Godin, L. (eds) *Channel Flow, Ductile Extrusion and Exhumation in Continental Collision Zones. Geological Society, London, Special Publications* **268**, 39–70.

Law, R. D., Searle, M. P. & Simpson, R. L. 2004. Strain, deformation temperatures and vorticity of flow at the top of the Greater Himalayan Slab, Everest Massif, Tibet. *Journal of the Geological Society, London* **161**, 305–20.

Law, R. D., Searle, M. P. & Godin, L. (eds) 2006. *Channel flow, ductile extrusion and exhumation in continental collision zones. Geological Society, London, Special Publication* **268**. 620 pp.

Le Breton, N. & Thompson, A. B. 1988. Fluid-absent (dehydration) melting of biotite in metapelites in the early stages of crustal anatexis. *Contributions to Mineralogy and Petrology* **99**, 226–37.

https://doi.org/10.1017/S175569100901617X Published online by Cambridge University Press

LeFort, P. 1975. Himalayas the Collided Range – Present Knowledge of Continental Arc. *American Journal of Science* **A275**, 1–44.

LeFort, P. 1981. Manaslu Leucogranite – a Collision Signature of the Himalaya; a Model for its Genesis and Emplacement. *Journal of Geophysical Research* **86**, 545–68.

Murphy, M. A. & Harrison, T. M. 1999. Relationship between leucogranites and the Qomolangma detachment in the Rongbuk Valley, south Tibet. *Geology* **27**, 831–4.

Nelson, K. D., Zhao, W., Brown, L. D., Kuo, J., Che, J., Liu, X., Klemperer, S. L., Makovsky, Y., Meissner, R., Mechie, J., Kind, R., Wenzel, F., Ni, J., Nabelek, J., Chen, L., Tan, H., Wei, W., Jones, A. G., Booker, J., Unsworth, B., Kidd, W. S. F., Hauck, M., Alsdorf, D., Ross, A., Cogan, M., Wu, C., Sandvol, E. A. & Edwards, M. A. 1996. Partially molten middle crust beneath southern Tibet; synthesis of Project INDEPTH results. *Science* **274**, 1684–8.

Noble, S. R. & Searle, M. P. 1995. Age of Crustal Melting and Leucogranite Formation from U–Pb Zircon and Monazite Dating in the Western Himalaya, Zanskar, India. *Geology* **23**, 1135–8.

Parrish, R. R. 1990. U–Pb dating of monazite and its application to geological problems. *Canadian Journal of Earth Sciences* **27**, 1431–50.

Parrish, R. R., Gough, S. J., Searle, M. P. & Waters, D. J. 2006. Plate velocity exhumation of ultrahigh-pressure eclogites in the Pakistan Himalaya. *Geology* **34**, 989–92.

Patiño Douce, A. E. & Harris, N. B. W. 1998. Experimental constraints on Himalayan anatexis. *Journal of Petrology* **39**, 689–710.

Petö, P. 1976. An experimental investigation of melting relations involving muscovite and paragonite in the silica-saturated portion of the system K_2O–Na_2O–Al_2O_3–SiO_2–H_2O to 15 kb total pressure. *Progress in Experimental Petrology* **3**, 41–5.

Pinet, C. & Jaupart, C. 1987. A thermal model for the distribution in space and time of Himalayan granites. *Earth and Planetary Science Letters* **84**, 87–99.

Priestley, K., Jackson, J. & McKenzie, D. 2008. Lithospheric structure and deep earthquakes beneath India, the Himalaya and southern Tibet. *Geophysical Journal International* **172**, 345–62.

Prince, C., Harris, N. B. W. & Vance, D. 2001. Fluid-enhanced melting during prograde metamorphism. *Journal of the Geological Society, London* **158** (2), 233–41.

Rai, S. S., Priestley, K., Gaur, V. K., Mitra, S., Singh, M. P. & Searle, M. P. 2006. Configuration of the Indian Moho beneath the NW Himalaya and Ladakh. *Geophysical Research Letters* **33**, L15308.

Rowley, D. B. 1996. Age of initiation of collision between India and Asia: A review of stratigraphic data. *Earth and Planetary Science Letters* **145**, 1–13.

Scaillet, B., France-Lanord, C. & LeFort, P. 1990. Badrinath–Gangotri Plutons (Garhwal, India) – Petrological and Geochemical Evidence for Fractionation Processes in a High Himalayan Leucogranite. *Journal of Volcanology and Geothermal Research* **44**, 163–88.

Scaillet, B., Pecher, A., Rochette, P. & Champenois, M. 1995. The Gangotri Granite (Garhwal Himalaya) – Laccolithic Emplacement in an Extending Collisional Belt. *Journal of Geophysical Research – Solid Earth* **100**, 585–607.

Scaillet, B., Holtz, F., Pichavant, M. & Schmidt, M. 1996. Viscosity of Himalayan leucogranites: Implications for mechanisms of granitic magma ascent. *Journal of Geophysical Research – Solid Earth* **101**, 27691–9.

Scaillet, B. & Searle, M. P. 2006. Mechanisms and timescales of felsic magma segregation, ascent and emplacement in the Himalaya. *In* Law, R. D., Searle, M. P. & Godin, L. (eds) *Channel Flow, Ductile Extrusion and Exhumation in Continental Collision Zones. Geological Society, London, Special Publications* **268**, 293–308. Bath, UK: The Geological Society Publishing House.

Schärer, U. 1984. The effect of initial ^{230}Th disequilibrium on young U–Pb ages: the Makalu case, Himalaya. *Earth and Planetary Science Letters* **67**, 191–204.

Schulte-Pelkum, V., Monsalve, G., Sheehan, A., Pandey, M. R., Sapkota, S., Bilham, R. & Wu, F. 2005. Imaging the Indian subcontinent beneath the Himalaya. *Nature* **435**, 1222–5.

Searle, M. P. 1999a. Emplacement of Himalayan leucogranites by magma injection along giant sill complexes: examples from the Cho Oyu, Gyachung Kang and Everest leucogranites (Nepal Himalaya). *Journal of Asian Earth Sciences* **17**, 773–83.

Searle, M. P. 1999b. Extensional and compressional faults in the Everest–Lhotse massif, Khumbu Himalaya, Nepal. *Journal of the Geological Society, London* **156**, 227–40.

Searle, M. P. 2003. *Geological Map of the Mount Everest massif, Nepal – South Tibet Himalaya.* Scale 1:100,000. Oxford: Oxford University.

Searle, M. P. 2007. *Geological Map of the Mount Everest–Makalu region Nepal – South Tibet Himalaya.* Scale 1:100,000. Oxford: Oxford University.

Searle, M. P., Cooper, D. J. W. & Rex, A. J. 1988. Collision tectonics of the Ladakh–Zanskar Himalaya. *Philosophical Transactions of the Royal Society, London* **A326**, 117–50.

Searle, M. P., Pickering, K. T. & Cooper, D. J. W. 1990. Restoration and evolution of the intermontane Indus molasse basin, Ladakh Himalaya, India. *Tectonophysics* **174**, 301–14.

Searle, M. P., Crawford, M. B. & Rex, A. J. 1992. Field Relations, Geochemistry, Origin and Emplacement of the Baltoro Granite, Central Karakoram. *Transactions of the Royal Society of Edinburgh: Earth Sciences* **83**, 519–38.

Searle, M. P., Metcalfe, R. P., Rex, A. J. & Norry, M. J. 1993. Field relations, petrogenesis and emplacement of the Bhagirathi leucogranite, Garhwal Himalaya. *In* Treloar, P. J. & Searle, M. P. (eds) *Himalayan Tectonics. Geological Society, London, Special Publications* **74**, 429–44. Bath, UK: The Geological Society Publishing House.

Searle, M. P., Parrish, R. R., Hodges, K. V., Hurford, A. J., Ayres, M. W. & Whitehouse, M. J. 1997. Shisha Pangma leucogranite, south Tibetan Himalaya: Field relations, geochemistry, age, origin, and emplacement. *Journal of Geology* **105**, 295–317.

Searle, M. P., Waters, D. J., Dransfield, M. W., Stephenson, B. J., Walker, J. D., Walker, C. B. & Rex, D. C. 1999a. Thermal and mechanical models for the structural evolution of the Zanskar High Himalaya. *In* MacNiocall, C. & Ryan, P. D. (eds) *Continental Tectonics. Geological Society, London, Special Publications* **164**, 139–56. Bath, UK: The Geological Society Publishing House.

Searle, M. P., Noble, S. R., Hurford, A. J. & Rex, D. C. 1999b. Age of crustal melting, emplacement and exhumation history of the Shivling leucogranite, Garhwal Himalaya. *Geological Magazine* **136**, 513–25.

Searle, M. P., Simpson, R. L., Law, R. D., Parrish, R. R. & Waters, D. J. 2003. The structural geometry, metamorphic and magmatic evolution of the Everest massif, High Himalaya of Nepal – South Tibet. *Journal of the Geological Society, London* **160**, 345–66.

Searle, M. P., Law R. D. & Jessup, M. J. 2006. Crustal structure, restoration and evolution of the Greater Himalaya in Nepal-South Tibet; implications for channel flow and ductile extrusion of the middle crust. *In* Law, R. D., Searle, M. P. & Godin, L. (eds) *Channel Flow, Ductile Extrusion and Exhumation in Continental Collision Zones. Geological Society, London, Special Publications* **268**, 355–78. Bath, UK: The Geological Society Publishing House.

Searle, M. P., Law, R. D., Godin, L., Larson, K., Streule, M. J., Cottle, J. M. & Jessup, M. J. 2008. Defining the Himalayan Main Central Thrust in Nepal. *Journal of the Geological Society, London* **165**, 523–34.

Searle, M. P. & Godin, L. 2003. The South Tibetan detachment and the Manaslu Leucogranite; a structural reinterpretation and restoration of the Annapurna–Manaslu Himalaya, Nepal. *Journal of Geology* **111**, 505–23.

Searle, M. P. & Rex, A. J. 1989. Thermal-Model for the Zanskar Himalaya. *Journal of Metamorphic Geology* **7**, 127–34.

Searle, M. P. & Szulc, A. G. 2005. Channel flow and ductile extrusion of the high Himalayan slab – the Kangchenjunga–Darjeeling profile, Sikkim Himalaya. *Journal of Asian Earth Sciences* **25**, 173–85.

Simpson, R. L., Parrish, R. R., Searle, M. P. & Waters, D. J. 2000. Two episodes of monazite crystallization during metamorphism and crustal melting in the Everest region of the Nepalese Himalaya. *Geology* **28**, 403–6.

Stevens, G., Clemens, J. D. & Droop, G. T. R. 1997. Melt production during granulite facies anatexis: experimental data from 'primitive' metasedimentary protoliths. *Contributions to Mineralogy and Petrology* **128**, 352–70.

Thimm, K. A., Parrish, R. R., Hollister, L. S., Grujic, D., Klepeis, K. & Dorji, T. 1999. New U–Pb data from the Lesser and Greater Himalayan sequences in Bhutan. *Journal of Conference Abstracts* **4**, 57.

Tilmann, F., Ni, J., Hearn, T., Ma, Y. S., Rapine, R., Kind, R., Mechie, J., Saul, J., Haines, S., Klemperer, S., Brown, L., PanAnont, P., Ross, A., Nelson, K. D., Guo, J., Zhao, W. & INDEPTH III Seismic Team. 2003. Seismic imaging of the downwelling Indian lithosphere beneath central Tibet. *Science* **300**, 1424–7.

Treloar, P. J., O'Brien, P. J., Parrish, R. R. & Khan, M. a. 2003. Exhumation of Tertiary coesite-bearing eclogites from the

https://doi.org/10.1017/S175569100901617X Published online by Cambridge University Press

Pakistan Himalaya. *Journal of the Geological Society, London* **160**, 367–76.

Unsworth, M. J., Jones, A. G., Wei, W., Marquis, G., Gokarn, S. G., Spratt, J. E. & INDEPTH-MT Team. 2005. Crustal rheology of the Himalaya and Southern Tibet inferred from magnetotelluric data. *Nature* **438**, 78–81.

Vance, D. & Harris, N. 1999. Timing of prograde metamorphism in the Zanskar Himalaya. *Geology* **27**, 395–8.

Vielzeuf, D. & Holloway, J. R. 1988. Experimental determination of the fluid-absent melting relations in the pelitic system; consequences for crustal differentiation. *Contributions to Mineralogy and Petrology* **98**, 257–76.

Viskupic, K., Hodges, K. V. & Bowring, S. A. 2005. Timescales of melt generation and the thermal evolution of the Himalayan metamorphic core, Everest region, eastern Nepal. *Contributions to Mineralogy and Petrology* **149**, 1–21.

Viskupic, K. & Hodges, K. V. 2001. Monazite–xenotime thermochronometry: methodology and an example from the Nepalese Himalaya. *Contributions to Mineralogy and Petrology* **141**, 233–47.

Walker, J. D., Martin, M. W., Bowring, S. A., Searle, M. P., Waters, D. J. & Hodges, K. V. 1999. Metamorphism, melting, and extension: Age constraints from the High Himalayan Slab of southeast Zanskar and northwest Lahaul. *Journal of Geology* **107**, 473–95.

Walker, C. B., Searle, M. P. & Waters, D. J. 2001. An integrated tectonothermal model for the evolution of the High Himalaya in western Zanskar with constraints from thermobarometry and metamorphic modeling. *Tectonics* **20**, 810–33.

Wei, W., Unsworth, M., Jones, A., Booker, J., Tan, H., Nelson, D., Chen, L., Li, S., Solon, K., Bedrosian, P., Jin, S., Deng, M., Ledo, J., Kay, D. & Roberts, B. 2001. Detection of widespread fluids in the Tibetan crust by magnetotelluric studies. *Science* **292**, 716–18.

Weinberg, R. F. & Searle, M. P. 1999. Volatile-assisted intrusion and autometasomatism of leucogranites in the Khumbu Himalaya, Nepal. *Journal of Geology* **107**, 27–48.

White, R. W., Powell, R. & Holland, T. J. B. 2001. Calculation of partial melting equilibria in the system Na_2O–CaO–K_2O–FeO–MgO–Al_2O_3–SiO_2–H_2O (NCKFMASH). *Journal of Metamorphic Geology* **19** (2), 139–53.

Whittington, A. G., Harris, N. B. W. & Baker, J. 1998. Low-pressure crustal anatexis: the significance of spinel and cordierite from metapelitic assemblages at Nanga Parbat, northern Pakistan. *In* Treloar, P. J. & O'Brien, P. J. (eds) *What Drives Metamorphism and Metamorphic Reactions? Geological Society, London, Special Publications* **138**, 183–98. Bath, UK: The Geological Society Publishing House.

Whittington, A. G., Harris, N. B. W. & Butler, R. W. H. 1999. Contrasting anatectic styles at Nanga Parbat, northern Pakistan. *In* Macfarlane, A., Sorkhabi, R. B. & Quade, J. (eds) *Himalaya and Tibet: Mountain Roots to Mountain Tops. Geological Society of America, Special Paper* **328**, 129–44.

Whittington, A. G. & Treloar, P. J. 2002. Crustal anatexis and its relation to the exhumation of collisional orogenic belts, with particular reference to the Himalaya. *Mineralogical Magazine* **66**, 53–91.

Wu, C., Nelson, K. D, Wortman, G., Samson, S., Yue, Y., Li, J., Kidd, W. S. F. & Edwards, M. A. 1998. Yadong cross-structure and South Tibetan Detachment in the east central Himalaya. *Tectonics* **17**, 28–45.

Zeitler, P. K., Koons, P. O., Bishop, M. P., Chamberlain, C. P., Craw, D., Edwards, M. A., Hamidullah, S., Jan, M. Q., Khan, M. A., Khattak, M. U. K., Kidd, W. S. F., Mackie, R. L., Meltzer, A. S., Park, S. K., Pecher, A., Poage, M. A., Sarker, G., Schneider, D. A., Seeber, L. & Shroder, J. F. 2001a. Crustal reworking at Nanga Parbat, Pakistan: Metamorphic consequences of thermal-mechanical coupling facilitated by erosion. *Tectonics* **20**, 712–28.

Zeitler, P. K., Meltzer, A. S., Koons, P. O., Craw, D., Hallet, B., Chamberlain, C. P., Kidd, W. S. F., Park, S. K., Seeber, L., Bishop, M. & Shroder, J. 2001b. Erosion, Himalayan geodynamics and the Geomorphology of metamorphism. *GSA Today* **11** (January) 4–9.

Zhang, H. F., Harris, N. B. W., Parrish, R. R., Kelley, S., Zhang, L., Rogers, N., Argles, T. & King, J. 2004. Causes and consequences of protracted melting of the mid-crust exposed in the North Himalayan antiform. *Earth and Planetary Science Letters* **228**, 195–212.

Zhu, B., Kidd, W. S. F., Rowley, D. B., Currie, B. S. & Shafique, N. 2005. Age of initiation of the India–Asia collision in the east-central Himalaya. *Journal of Geology* **113**, 265–85.

MS received 11 December 2007. Accepted for publication 13 March 2008 (Stellenbosch); 15 January 2009 (RSE).

https://doi.org/10.1017/S175569100901617X Published online by Cambridge University Press